Numerical Simulation of Low Supersonic
Flow Around a Sphere*

ZHENG Zhi-Chu (郑之初), TANG An-Min (唐安民) and LIN Tong-Ji (林同骥)

(*Institute of Mechanics, Academia Sinica, Beijing 100080, PRC*)

Abstract   The controlled equations defined in a physical plane are changed into those in a computational plane with coordinate transformations suitable for different Mach number M, The computational area is limited in the body surface and in the vicinities of detached shock wave and sonic line. Thus the area can be greatly cut down when the shock wave moves away from the body surface as $M_\infty \rightarrow 1$. Highly accurate, total variation diminishing (TVD) finite-difference schemes are used to calculate the low supersonic flowfield around a sphere. The stand-off distance, location of sonic line, etc. are well comparable with experimental data. The long pending problem concerning a flow passing a sphere at $1.3 \geqslant M_\infty > 1$ has been settled, and some new results on $M_\infty = 1.05$ have been presented

Keywords: sphere, low supersonic flow, detached shock wave, sonic line, forward flowfield.

1 Introduction

The study on the high supersonic flow of a sphere began in the 1950s. Since then considerable experimental and computational results on $1.2 \leqslant M_\infty < \infty$ have been accumulated[1-3].   Later people's interest has gradually been directed to low supersonic and transonic flows around a sphere. Summing up the laws of the variation of shock wave stand-off distance and sonic point location with the changing M_∞, Ref. [4] pointed out that when $M_\infty \geqslant 1.5$, the results by different approaches agreed well with each other; in other words, the theoretical calculations coincided with the experimental results. However, there were great discrepancies between the results of experiments and empirical formulae at $M_\infty < -1.3$, especially at $M_\infty \rightarrow 1$. Take sonic line at $M_\infty = 1$ as an example, in Ref. [5], it extends forward, in Ref. [6] it goes backward near the body surface, whereas in Ref. [7] it moves backward away from the body surface, as plotted in Fig. 1(a)—(c). At that time it was hard to say which of the three was closest to the reality. The problem of how to calculate the supersonic flow around a sphere at $1.3 \geqslant M_\infty > 1$ has been an important topic in the realm of fluid mechanics since it was raised in the middle of the 1970s.

The recent studies are concentrated on the flowfield structure with viscosity. An idea

to take viscous influence into consideration is to divide the flowfield of a sphere into two parts, i.e. the forward flowfield (area I) and the backward flowfield (area II)[8]. Their boundary passes through the separation point in the body surface. In this paper, we are focusing on area I because its solution is the foundation for the viscous flow and at the same time it 's the key point to the research.

Before the 1980s the solutions of supersonic and low supersonic ideal gas flows in area I were classified into the following three catalogues: (i) classical method presented by Belotserkovskii[3] and Van Dyke[1], (ii) full potential equations method, such as shock wave capture method presented by Shankar[9], and (iii) Euler equation method, namely, the time-dependent method. With various dispersion formats, there formed different schemes, such as the MacCormack method, AF method, vector method. Flow field around a sphere could be calculated up to $M_\alpha > 1.08$ using these methods, and flow parameters, such as distribution, pressure contours between detacked shock wave and body surface were obtained besides the detached shock wave and sonic line.

Based on experiments and theoretical analysis this paper suggests that the main difficulty in calculating supersonic spherical flow at $M_\infty > 1$ originates in the fact that the flow parameters change very unevenly in the flowfield when the detached shock wave takes the shape of a straight line and moves away from the body surface by degrees. Hence, both fairly dense grids and highly accurate schemes are required lest minor errors may accumulate leading to numerical dispersion. Therefore, we propose (i) to select proper curvilinear coordinate in order that the computational area at different M_∞ is limited in the vicinities of the detached shock wave, sonic line and body surface so as to greatly reduce the computational area, (ii) to change the controlled equations defined in a physical plane into those in a computational plane with suitable coordinate transformation, and (iii) to solve the flowfield at $M_\alpha > 1$ from Euler's equation with highly accurate TVD finite-difference scheme designed to compute hyperbolic conservative equations presented by Harten[10].

Generally, compared with wind tunnel, the ballistic range facilities can better reveal the real situation of shock wave stand-off distance and its shape, especially for the backward flowfield structure and wave series. A ballistic range with different Mach number M_r and Reynolds number Re was designed and used to demonstrate the transonic flowfield around a sphere. Photographs were taken at $M_\infty = 0.8$—1.2 and $Re_d < 10^6$ to verify the numerical simulations.

2 Basic Equations

An aximystric, steady, adiabat supersonic flow around a sphere is presumed. Its controlled equations can be written as

$$\frac{\partial U}{\partial t} + \frac{\partial F}{\partial x} + \frac{\partial G}{\partial y} + H = 0, \tag{1}$$

in which

$$U = (\rho, \ \rho u, \ \rho v, \ e)^T,$$

$$G = (\rho v, \ \rho u v, \ \rho v^2 + p, \ (e + p) v)^T,$$

$$F = (\rho u, \ \rho u^2 + p, \ \rho u v, \ (e + p) u)^T.$$

Here, ρ, p, u, v, e, t represent fluid density, pressure, x-direction component, y-direction component, intrinsic energy per unit volume and time, respectively. All variables in equations are normalized with respect to the following free stream values and the bar is ignored for convenience:

$$\bar{\rho} = \rho \left/ \frac{p_\infty}{a_\infty^2} \right., \quad \bar{p} = p/p_\infty, \quad \bar{e} = e/p_\infty, \quad \bar{t} = t \left/ \frac{R}{a_\infty} \right.,$$

$$\bar{u} = u/a_\infty, \quad \bar{v} = v/a_\infty, \quad \bar{x} = x/R, \quad \bar{y} = y/R,$$

where p_∞, a_∞ and R represent free-stream pressure, sound speed and sphere radius. A coordinate transformation is introduced to simplify computation,

$$x = x(\xi, \eta), \quad y = y(\xi, \eta). \tag{2}$$

The controlled equations defined in physical plane (x, y) are changed into those in a computational plane (ξ, η). The equations after transformation are

$$\frac{\partial \tilde{U}}{\partial t} + \frac{\partial \tilde{F}}{\partial \xi} + \frac{\partial \tilde{G}}{\partial \eta} + \tilde{H} = 0, \tag{3}$$

in which $\tilde{U} = U/J$, $\tilde{F} = (\xi_x F + \xi_y G)/J$, $\tilde{G} = (\eta_x F + \eta_y G)/J$, $\tilde{H} = H/J$, $J = \xi_x \eta_y - \xi_y \eta_x$.

Usually, whether the numerical calculations converge or not is determined by coordinate transformation (2) in some degree. Grids in (ξ, η) plane must be orthogonal and even-distributed in order to ensure rapid convergence.

3 Solving of Equations

3.1 Explicit TVD Scheme

The following explicit TVD schemes are constructed to solve nonhomogeneous conservative equations[3]:

$$\tilde{U}_{i,j}^{n+1} = \tilde{U}_{i,j}^n - \lambda_\xi [M_{i+\frac{1}{2},j}^n - M_{i-\frac{1}{2},j}^n] - \lambda_\eta [N_{i,j+\frac{1}{2}}^n - N_{i,j-\frac{1}{2}}^n] - \Delta t \, \tilde{H}_{i,j}^n, \tag{4}$$

where $\lambda_\xi = \Delta t/\Delta \xi$, $\lambda_\eta = \Delta t/\Delta \eta$,

$$M_{i+\frac{1}{2},j}^n = \frac{1}{2} \left(\tilde{F}_{i,j}^n + \tilde{F}_{i+1,j}^n + \frac{1}{\lambda_\xi} R_{\xi i \frac{1}{2},j} \cdot \beta_{\xi i + \frac{1}{2} j} \right), \tag{5}$$

$$\beta^l_{\xi i,\frac{1}{2},j} = g^l_{\xi i\, j} + g^l_{\xi i+1\, j} - Q(v^l_{\xi i+\frac{1}{2},j} + \gamma^l_{\xi i+\frac{1}{2}\, j}) \cdot \alpha^l_{\xi i+\frac{1}{2},j}, \tag{6}$$

$$g^l_{\xi i\, j} = S_\xi \max\left[0, \min\left(\sigma|g^l_{\xi i+\frac{1}{2},j}|, \sigma S_\xi \tilde{g}_{\xi i-\frac{1}{2}\, j}, \frac{1}{2}|\tilde{g}^l_{\xi i-\frac{1}{2},j} + \tilde{g}^l_{\xi i+\frac{1}{2}\, j}|\right)\right], \tag{7}$$

$$\tilde{g}^l_{\xi i+\frac{1}{2}\, j} = \frac{1}{2}[Q(v^l_{\xi\, i+\frac{1}{2}\, j}) - (v^l_{\xi\, i+\frac{1}{2},j})^2]\,\alpha^l_{\xi i+\frac{1}{2},j}, \tag{8}$$

$$S_\xi = \operatorname{sign}(\tilde{g}^l_{\xi i+\frac{1}{2}\, j}). \tag{9}$$

$$v^l_{\xi i+\frac{1}{2}\, j} = \lambda_\xi\, a^l_{\xi i+\frac{1}{2}\, j}, \tag{10}$$

$$\gamma^l_{\xi i+\frac{1}{2}\, j} = \begin{cases} (g^l_{\xi\, i+1,j} - g^l_{\xi\, i\, j})/\alpha^l_{\xi\, i+\frac{1}{2}\, j} & \alpha^l_{\xi\, i+\frac{1}{2},j} \neq 0, \\ 0 & \alpha^l_{\xi\, i+\frac{1}{2},j} = 0, \end{cases} \tag{11}$$

$$\alpha^l_{\xi i+\frac{1}{2}\, j} = R^{-1}_{\xi\, i+\frac{1}{2}\, j}(U^n_{i+1\, j} - U^n_{i\, j})\left/\frac{1}{2}(J_{i,j} + J_{i+1\, j}),\right. \tag{12}$$

where α_ξ is the eigenvector of $\tilde{A} = \partial\tilde{F}/\partial\tilde{U}$, R_ξ is the matrix whose columns are eigenvectors of $\tilde{A}$ and R^{-1} is the inverse matrix of R_ξ; its expression can be found in Ref. [12].

Similarly,

$$N^n_{i\, j+\frac{1}{2}} = \frac{1}{2}\left(\tilde{G}^n_{i\, j} + \tilde{G}^n_{i,j+1} + \frac{1}{\lambda_\eta}R_\eta\,\beta_{\eta\, i,j+\frac{1}{2}}\right), \tag{13}$$

$$\beta^l_{\eta i\, j+\frac{1}{2}} = g^l_{\eta i,j} + g^l_{\eta i,j+1} - Q(v^l_{\eta i,j+\frac{1}{2}} + \gamma^l_{i,j+\frac{1}{2}})\,\alpha^l_{\eta i\, j+\frac{1}{2}}, \tag{14}$$

$$g^l_{\eta i\, j} = S_\eta \max\left[0, \min\left(\sigma|\tilde{g}^l_{\eta i,j+\frac{1}{2}}|, \sigma S_\eta \tilde{g}^l_{\eta i,j-\frac{1}{2}},\right.\right.$$
$$\left.\left.\frac{1}{2}|\tilde{g}^l_{\eta i\, j-\frac{1}{2}} + \tilde{g}^l_{\eta i,j+\frac{1}{2}}|\right)\right], \tag{15}$$

$$\tilde{g}^l_{\eta i\, j+\frac{1}{2}} = \frac{1}{2}[Q(v^l_{\eta i\, j+\frac{1}{2}}) - (v^l_{\eta i\, j+\frac{1}{2}})^2]\,\alpha^l_{\eta i,j+\frac{1}{2}}, \tag{16}$$

$$S_\eta = \operatorname{sign}(\tilde{g}^l_{\eta i\, j+\frac{1}{2}}). \tag{17}$$

$$v^l_{\eta i\, j+\frac{1}{2}} = \lambda_\eta\, a^l_{\eta i\, j+\frac{1}{2}}. \tag{17'}$$

$$\gamma^l_{\eta i\, j+\frac{1}{2}} = \begin{cases} (g^l_{\eta i\, i+1} - g^l_{\eta i\, j})/\alpha^l_{\eta i\, j+\frac{1}{2}}, & \alpha^l_{\eta i,j+\frac{1}{2}} \neq 0 \\ 0, & \alpha^l_{\eta i\, j+\frac{1}{2}} = 0 \end{cases} \tag{18}$$

$$\alpha^l_{\eta i\, j+\frac{1}{2}} = R^{-1}_{\eta i\, j+\frac{1}{2}}(U^n_{i\, j+1} - U^n_{i\, j})\left/\frac{1}{2}(J_{i,j} + J_{i\, j+1}),\right. \tag{19}$$

where α_η is the eigenvector of $\tilde{B} = \partial\tilde{G}/\partial\tilde{U}$, R_η is the matrix whose columns are eigenvectors of $\tilde{B}$, and R^{-1}_η is the inverse matrix of R_η. In order to satisfy the entropy condition, let

$$Q(x) = \begin{cases} \dfrac{x^2 + \varepsilon^2}{2\varepsilon} & |x| < \varepsilon, \\ |x| & |x| \geqslant \varepsilon. \end{cases} \tag{20}$$

In the calculation, arithmetic average values are taken as centre average values. Changeable time steps are used to fasten the iterations according to Refs. [13].

$$\overline{\Delta t} = \Delta t / (1 + \sqrt{J}).\tag{21}$$

Yu[14] proved that one-dimensional TVD scheme has the maximum precision when $\sigma = 2$. So $\sigma = 2$ is assumed in this paper. Nonhomogeneous items in symmetric axis $y = 0$ are treated with L' Hospital's principle.
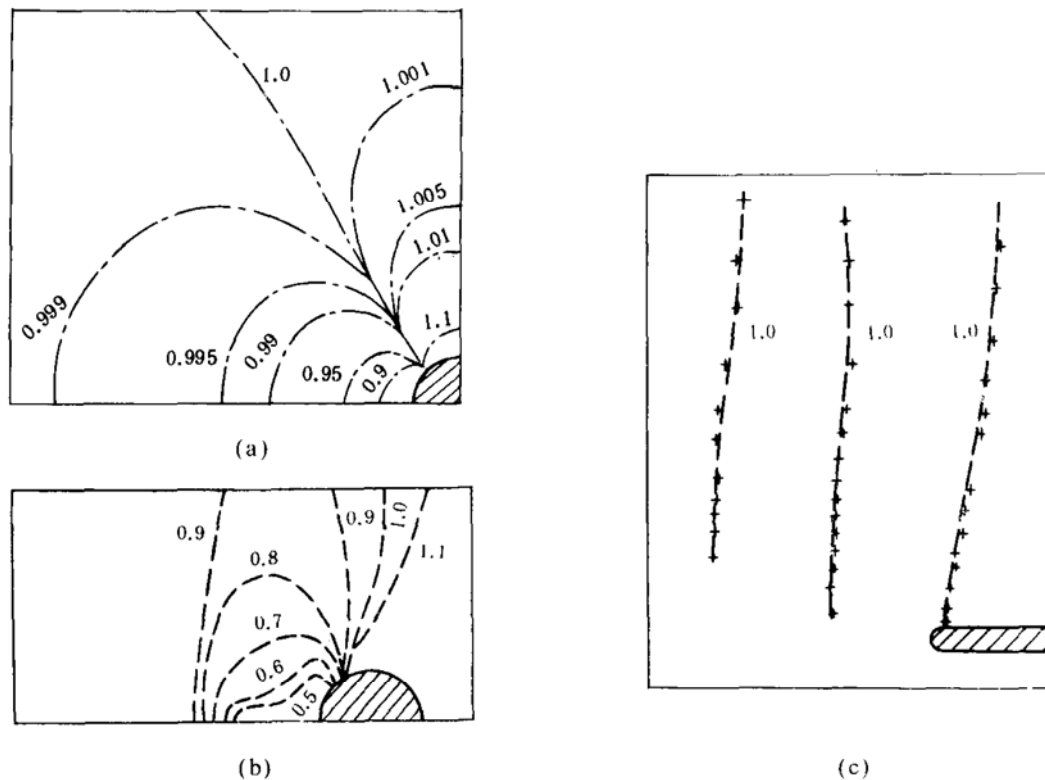

(a)

(b)

(c)

Fig. 1. Three results of sonic line with $M_\infty = 1$ (a) Result obtained by Lin, T J, (b) result obtained by Beloserkovskii,   (c) result obtained by Hsien, T
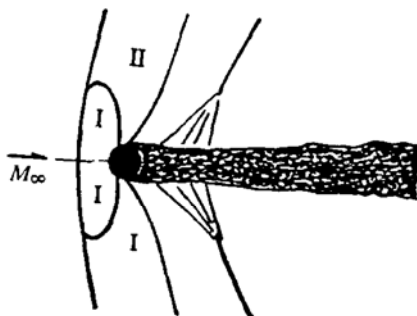

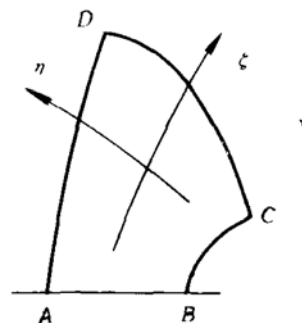Fig. 2. Illustration of division of the computational area.

Fig. 3. Illustration of curvilinear coordinate and boundaries of computational area.

3.2 Grids Generation

The curvilinear coordinate (ξ, η) and four boundaries of the computational area are shown in Fig.3, where $\xi = 0$ AB is the symmetric boundary, $\xi = \xi_M$ CD is the out-flow

boundary, $\eta = 0$ BC is the body surface and $\eta = 1$ AD is the entrance boundary. To acquire a computational area as small as possible, curves AD and CD should have similar shape of detached shock wave and sonic line, respectively. Their shapes are functions of free-stream Mach number M_∞. Through an analysis of the experimental results in ballistic ranges at different Mach number M_∞ the following coordinate transformations are chosen:

$$x = -f \cos k, \quad y = -f \sin k, \tag{22}$$

where

$$f = 1 + \eta_1 [s(k) \cdot G(\xi, \eta) - 1] \tag{23}$$

$$s(k) = R_0(1 + \varepsilon)/(1 + \varepsilon \cos k), \quad \varepsilon = 1.4/(M_\infty^2 - 1)^{0.485},$$

$$R_0 = 1 + 0.46 \varepsilon^{1.18}, \tag{24}$$

$$k = \xi_1 / g(\eta_1) \tag{25}$$

$$g(\eta_1) = A_2 \eta_1^2 + A_1 \eta_1 + 1, \tag{26}$$

$$A_2 = f_0 - A_1 - 1,$$

$$A_1 = [f_2 - 1 - (f_0 - 1) s_1^2]/s_1(1 - s_1),$$

$$G(\xi, \eta) = 1 + \sigma \varepsilon \cos k \tag{27}$$

$$\xi_1 = \frac{\pi}{2} \left[\frac{\sqrt{1 + \alpha(2 + \alpha)\xi} - 1}{\alpha} \right], \tag{28}$$

$$\eta_1 = \eta - \beta \sin 2\pi\eta. \tag{29}$$

When computing free-stream Mach number M_∞ ($M_\infty \geqslant 1.05$), we chose parameters as follows: $\alpha = 1, 2$, $\beta = 0.05$, $f_0 = 1.32$, $f_1 = 1.26$, $s_1 = 0.8$, $\sigma = 0.001$. Quite satisfactory grids are obtainable. The curvilinear coordinates, grids and computation results corresponding to $M_\infty = 1.1, 1.05$ are plotted in Figs. 4 and 5, respectively. Although the grid numbers increase when $M_\infty \to 1$, our scheme can achieve satisfactory results with fewer grids and less computation time.

3 3 Boundary Conditions

3.3 1 Entrance boundary AD. For supersonic free-stream, all upstream parameters P_∞, ρ_r, a_r, M_∞ are presumed.

3.3 2 Symmetric boundary AB. Values in this boundary can be calculated by mirror-image method.

3.3.3 Body surface boundary BC. In order that the arc coincident with body surface is a stream line, a mirror-image method in curvilinear coordinate form is adopted to calculate the values in this arc.
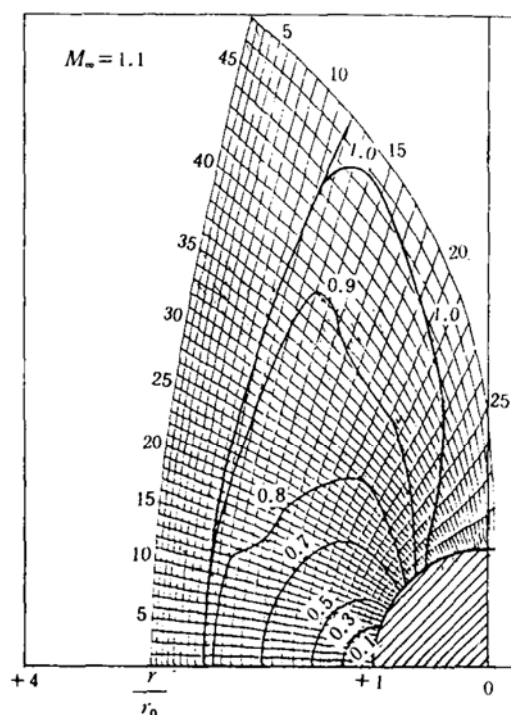
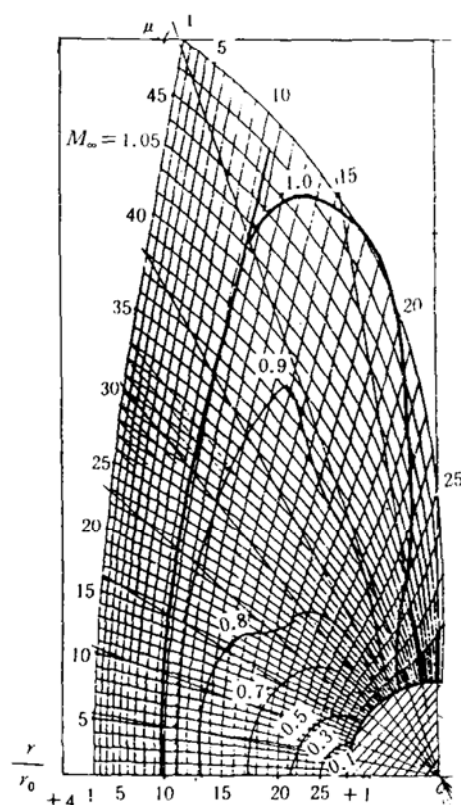Fig. 4. Mach contours and detached shock
wave with $M_\infty = 1.1$

Fig. 5. Mach contours and detached shock
wave with $M_r = 1.05$

3.3.4 Out-flow boundary CD. Assuming that the out-flow boundary has no effect on the location of sonic line, all values are first-order extrapolated.

3.4 Initial Conditions

Boundary AD should be obtained at first. With given M_∞, let $M_\infty^* < M_\infty$, put it into (24) and get the curve AD. For example let $M_\infty^* = 1.08$ when computing $M_\infty = 1.1$. Then fit a bow-shaped shock wave in an iso-η line. Curvilinear grids can be computed by expressions (22)—(29) when the grid number is given. Flowfield of shock wave layer can be calculated by intrapolation with behind-wave values and body surface values. Usually a small subsonic flowfield area near the stagnation point of sphere is assumed with other area being even flowfield having free-stream values. After several iterations, the subsonic area increases and finally reaches steady state.

3.5 Shock Wave Simulation

Because of the artificial viscosity term introduced, the calculated shock wave is a relatively wide layer. The flow parameters change from free-stream values to behind-wave values in this layer. In fact, shock wave is a very thin layer, so it is important to locate shock wave for precision requirements. The following formulae defined in meridian plane are chosen to simulate shock wave.

$$\frac{p_2}{p_\infty} = \frac{2\gamma}{\gamma+1}\left(M_\infty^2 \sin^2\beta - \frac{\gamma-1}{2\gamma}\right), \tag{30}$$

$$tg\ \alpha = \frac{ctg\ \beta \left(\sin^2 \beta - \frac{1}{M_\infty^2} \right)}{\frac{\gamma + 1}{2} - \left(\sin^2 \beta - \frac{1}{M_\infty^2} \right)} \ , \tag{31}$$

$$tg\ \alpha = \frac{v}{u} \ , \tag{32}$$

in which p_2 and β represent behind-wave pressure and shock wave angle, respectively. The shock wave is normal in symmetric axis, viz. $\beta = 90$. Substituting it into expression (30) yields $\frac{p_2}{p_\ell} = \frac{2\gamma}{\gamma + 1} \left(M_\infty^2 - \frac{\gamma - 1}{2\gamma} \right)$. Compared with calculated pressure values, the stand-off distance of shock wave can be obtained. Then using the following formula in Ref. [14]

$$tg\ \beta = \frac{\varepsilon + \cos\theta}{\sin\theta} \ , \tag{33}$$

we get β initial value and then insert it into expression (30) to obtain p_2/p_∞. Thus the initial shock wave location can be given. Putting β in expression (31), we obtain $tg\alpha_1$. Velocity components u, v corresponding to the initial shock wave location are utilized to calculate $tg\ \alpha_2$. Comparing $tg\alpha_1$ and $tg\alpha_2$, rectifying β till their difference is smaller than minor number μ, namely, $|tg\alpha_1 - tg\alpha_2| \leqslant \mu$, the shock wave location is obtained finally. The simulated shock waves are plotted in Figs. 4 and 5, respectively. It can be seen from the figures that flowfields behind simulated shock wave are well comparable with experimental results.

4   Conclusion and Discussion

The strategy presented in this paper enables us to calculate the supersonic flowfield around a sphere at $M_\infty > 1.5$ quickly and accurately. Similarly, the flowfield at $1.2 \geqslant M_\ell > 1.05$ can be calculated with enough precision and fastness if the coordinate transformations presented in this paper are adopted. As examples, here three grid schemes 19×27, 29×47, 29×47 are used to calculate the flow around a sphere at $M_\ell = 1.2$. 1.1 and 1.05. The results are shown in Figs. 4 and 5, respectively, from which we see that the grids numbers vary with M_∞; when $M_\infty = 1.2$, they can be immensely cut down while the precision is the same. As $M_\infty \to 1$, the grid numbers should be gradually increased. The coordinate transformations presented in this paper make the computational area include properly the detached shock wave, sonic line and body surface. Therefore, the computational area is much smaller and the computation time is greatly saved.

A continuous increase in gas velocity from symmetric axis of sphere to sonic line can be seen from the velocity distributions. But since they are far from both the body sur-

face and the detached shock wave so that the gas has a relatively slow acceleration, there are depressions in $0.8 - 0.9$ iso-M_∞ lines. It can be seen that longer distances are demanded when the local Mach number accelerates from 0.8 to 0.9 and 1.0 at $M_\infty \to 1$. This means that adjacent grid point ΔM_∞ should be very small and if grids are not dense enough, the errors may accumulate easily in iterations and finally lead to divergence of numerical results. The conventional numerical schemes require the flowfield to extend to infinity and need much more grids in order to get enough dense grids. That is why they meet difficulties in solving flowfield of a sphere when $M_\infty \to 1$.
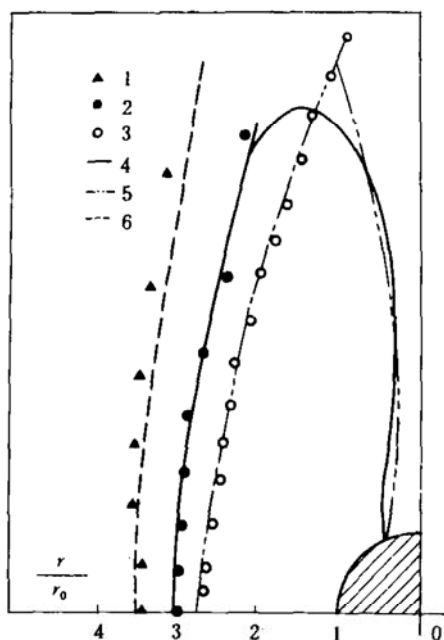

Fig. 6. Comparison of result of the current scheme and experimental data with $M_\infty = 1.1$.
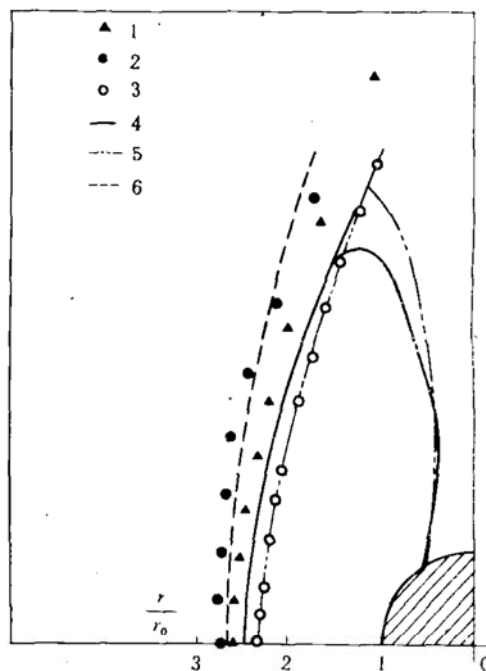
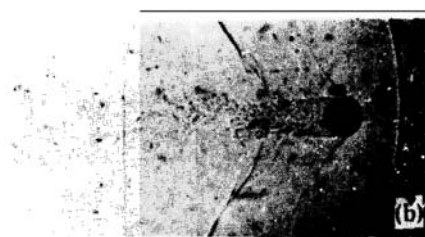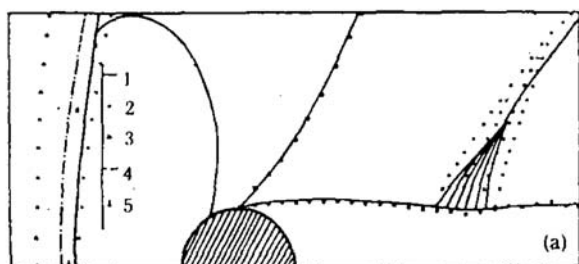Fig. 7. Comparison of result of the current scheme and experimental data with $M_\infty = 1.05$.

Fig. 8 (a) Comparison of backward flowfield result and experimental data with $M_\infty = 1.05$; (b) photograph of ballistic range for flowfield around a sphere with $M_\infty = 1.12$.

The shapes of detached shock wave and sonic line are characteristic marks of the flowfield around a sphere. Figs. 6 and 7 give a comparison between the results on detached shock waves and sonic lines at $M_\infty = 1.1$, 1.05 by our scheme, other methods and experiments. There are many numerical results when $M_\infty \geqslant 1.2$, but some numerical schemes are no longer applicable when $M_\infty \to 1$. Our scheme can calculate M_∞ as high as 1.05, and the results agree well with the one of ballistic range. The sonic lines at

$1.2 \geqslant M_\infty > 1.05$ are also plotted in Figs. 6 and 7. They start at sphere surface, extend to the stream direction at first, then move forward slowly departing from the body surface, and finally bend to the detached shock wave quickly when they approach it. In Ref. [15] the supersonic characteristic line methods were used to solve the backward flowfield with the calculated sonic lines as initial values. The calculated results on separated shock wave, base flow iso-pressure boundary and tail shock wave locations are well comparable with those of ballistic range, as shown in Fig. 8, indicating that the sonic line calculated with our scheme is in accordance with the reality of flow. From the comparison of the three sonic lines at $M_\infty = 1$ in Fig. 1 with ours, we think that the sonic line in Fig. 1(c) deviates from the real situation, the lines in Fig. 1(b) are consistent with our results in the near body flowfield and seem reasonable, whereas the line in Fig. 1(a) is convincing in farther flowfield, which can be explained physically as follows. The detached shock wave moves away from the body surface when $M_\infty \to 1$ and its departure velocity increases slower than gas velocity between the detached shock wave and body surface, so the sonic line inclines to the detached shock wave more quickly, leading the subsonic flowfield between detached shock wave and body surface to avoid tending to infinity. Thus we see that the flowfield around a sphere at $M_\infty \to 1$ can be solved numerically.

To sum up, our numerical simulation method can solve the flowfield around a sphere till $M_\infty \geqslant 1.05$ with smaller computational area and less computation time. It can be extended to solve low supersonic forward flowfield around hemisphere-compounds, sphere-cone compounds and blund body such as elliptic sphere and flat-headed cylinder, thus opening up a way for solving viscous backward flowfield.

References

1   Van Dyke, M D. & Gordon, H Y, NASA TR-1, 1959.
2   Antonov, A M & Hayes, W D, J. Appl Math. & Mech., 1966, (2):347.
3   Belotserkovskii, O M & Chushkin, P I, Basic Developments in Fluid Dynamics (ed. Holt, M.), 1965, 1:1.
4   Zheng, Z. C, Acta Aerodynamica Sinica (in Chinese), 1984, (3):98.
5   Lin, T J & Jia, Z. X., 1981 Proc. Indian Academy of Sci., Vol. 4, Part 3, pp. 315—345.
6   Belotserkovskii, O M, AD-AO71419, 1979, p.3
7   Hsien T, AIAA Paper, pp. 75—83.
8   Zheng, Z. C et al., Acta Mechanica Sinica (in Chinese), 1984, 16(3):234.
9   Shankar V, AIAA J., 1982, 20(11):1508.
10   Harten, A, J. Comput Phys., 1983, 49:357
11   Wu, Y X et al, Acta Aerodynamica Sinica (in Chinese), 1991, (4):387.
12   Pulhan, T H et al, AIAA Paper, 85-0360, 1985
13   Yee, H C & Harten A, AIAA Paper 85-1513, 1985.
14   Yu, X., J Numerical Methods & Computer Applications, 1987, (4):239.
15   Wu, Y X, Zheng, Z C & Lin, T J., Acta Mechanica Sinica (in Chinese), 1992, 24(6).